APL Materials

Epitaxial integration of high-mobility La-doped $BaSnO_3$ thin films with silicon

Cite as: APL Mater. **7**, 022520 (2019); https://doi.org/10.1063/1.5054810
Submitted: 03 September 2018 • Accepted: 16 October 2018 • Published Online: 22 January 2019

Zhe Wang, Hanjong Paik, Zhen Chen, et al.

Epitaxial integration of high-mobility La-doped $BaSnO_3$ thin films with silicon

Cite as: APL Mater. 7, 022520 (2019); doi: 10.1063/1.5054810
Submitted: 3 September 2018 • Accepted: 16 October 2018 •
Published Online: 22 January 2019

Zhe Wang,[1,a)] Hanjong Paik,[2,3,a)] Zhen Chen,[1] David A. Muller,[1,4] and Darrell G. Schlom[2,4,b)]

AFFILIATIONS

[1] School of Applied and Engineering Physics, Cornell University, Ithaca, New York 14853, USA
[2] Department of Materials Science and Engineering, Cornell University, Ithaca, New York 14853, USA
[3] Platform for the Accelerated Realization, Analysis, and Discovery of Interface Materials (PARADIM), Cornell University, Ithaca, New York 14853, USA
[4] Kavli Institute at Cornell for Nanoscale Science, Ithaca, New York 14853, USA

[a)] **Contributions:** Z. Wang and H. Paik contributed equally to this work.
[b)] **Author to whom correspondence should be addressed:** schlom@cornell.edu

ABSTRACT

La-doped $BaSnO_3$ has been epitaxially integrated with (001) Si using an $SrTiO_3$ buffer layer via molecular-beam epitaxy (MBE). A 254 nm thick undoped $BaSnO_3$ buffer layer was grown to enhance the mobility of the overlying La-doped $BaSnO_3$ layer. The x-ray diffraction rocking curve of the $BaSnO_3$ 002 peak has a full width at half maximum of 0.02°. At room temperature, the resistivity of the La-doped $BaSnO_3$ film is 3.6×10^{-4} Ω cm and the mobility is 128 $cm^2\ V^{-1}\ s^{-1}$ at a carrier concentration of 1.4×10^{20} cm^{-3}. These values compare favorably to those of La-doped $BaSnO_3$ films grown by all techniques other than MBE on single-crystal oxide substrates. Our work opens an exciting arena for integrating hyper-functional oxide electronics that make use of high-mobility oxide films with the workhorse of the semiconductor industry, silicon.

Recently there has been tremendous interest in La-doped $BaSnO_3$ because of its unusually high mobility at room temperature for a transparent conducting oxide. Mobilities in La-doped $BaSnO_3$ single crystals[1] and thin films[2] have reached 320 $cm^2\ V^{-1}\ s^{-1}$ and 183 $cm^2\ V^{-1}\ s^{-1}$, respectively. The high room-temperature mobility of La-doped $BaSnO_3$, in combination with its transparency at optical wavelength, ability to be heavily doped, and oxygen stability[1,3–6] makes it an exciting component for fabricating novel thermally stable devices including power electronics,[7,8] optoelectronic devices,[9–11] thermoelectric devices,[12] solar cells,[13] and field effect transistors.[14,15] Moreover, thanks to the structural and chemical compatibility of $BaSnO_3$ with functional perovskite oxides that show a plethora of novel and emergent properties, a heterostructure consisting of high-mobility La-doped $BaSnO_3$, and other perovskite oxides can potentially enrich the family of functionalities of all-oxide heterostructures and provide opportunities for hybrid devices by exploiting emergent phenomena of oxide interfaces and heterostructures.[16,17] For example, integration of high mobility La-doped $BaSnO_3$ with ferroelectrics such as Pb(Zr, Ti)O_3 can potentially realize devices including nonvolatile memories,[18] ferroelectric field-effect transistors,[19] low-power transistors that can beat the 60 mV/decade subthreshold slope limit of conventional semiconductors,[20] and hyper-sensitive temperature or pressure sensors.[21]

While rapid progress has been made on the growth of high-mobility $BaSnO_3$ thin films during the last few years,[1,2,22–28] most of the La-doped $BaSnO_3$ thin films have been grown on single-crystal oxide substrates which are currently limited to small size (typically no larger than 10 × 10 mm). Very limited work on La-doped $BaSnO_3$ thin films has been carried out on scalable substrates of industrial quality,[29] thus making it difficult to take advantage of the well-developed and efficient fabrication processes in the semiconductor industry.

Specifically, there is no report of growing La-doped $BaSnO_3$ films on the backbone of semiconductor industry, silicon.

The integration of functional oxides directly on silicon, however, is difficult due to the reactive nature of the (001) Si surface with oxygen to form an amorphous SiO_2 layer that can impede epitaxial growth. Furthermore, most oxides react with silicon. Due to the unknown free energy of $BaSnO_3$, we are unable to assess its thermodynamic stability in direct contact with silicon. We note, however, that the binary components of $BaSnO_3$—BaO and SnO_2—are both thermodynamically unstable in contact with silicon.[30] From a simple bond strength perspective, where energies are assigned to M—O bonds (where M is a cation), this would suggest that $BaSnO_3$ is unstable in direct contact with silicon.[31] The lack of thermodynamic stability does not, however, preclude epitaxial growth. The epitaxial growth of an unstable interface can sometimes be achieved at low temperature, e.g., room temperature as is used to form epitaxial BaO/Si[32] or CeO_2/Si interfaces,[33] both of which are thermodynamically unstable. Upon heating to about 650 °C, however, reaction is observed at these interfaces following the expectations of thermodynamics.[30,34–37]

To date, only a few oxides have been epitaxially grown directly on silicon. These include BeO,[38,39] MgO,[40,41] SrO,[36,42] BaO,[32,43] Sc_2O_3,[44] Y_2O_3,[45] ZrO_2,[46] HfO_2,[47] La_2O_3,[48] CeO_2,[33] Pr_2O_3,[49,50] Nd_2O_3,[51,52] Sm_2O_3,[53] EuO,[54,55] Gd_2O_3,[56–58] Dy_2O_3,[53] Ho_2O_3,[53] Er_2O_3,[58,59] Tm_2O_3,[60] Lu_2O_3,[61] Al_2O_3,[62] yttria-stabilized zirconia (YSZ),[63] yttria-stabilized hafnia (Y_2O_3-HfO_2),[64] (Ba, Sr)O,[36,43] (La, Y)$_2O_3$,[65] (Pr, Y)$_2O_3$,[66] (La, Lu)$_2O_3$,[67–69] $MgAl_2O_4$,[70] $SrTiO_3$,[71,72] $La_2Zr_2O_7$,[73] $SrHfO_3$,[74,75] Ba_2SiO_4,[37] and $La_2Hf_2O_7$.[76] Among these, $SrTiO_3$ is one of the most frequently used epitaxial buffer layers for the growth of functional oxides on (001) Si,[77] thanks to its relatively high crystalline quality on silicon[78–80] and its structural compatibility with various functional perovskite materials.[77,81]

Here we report growth of La-doped $BaSnO_3$ films on (001) Si using a $SrTiO_3$ buffer layer grown by molecular-beam epitaxy (MBE). The resulting La-doped $BaSnO_3$ film on silicon is epitaxial, with a room-temperature mobility of 128 $cm^2\ V^{-1}\ s^{-1}$ and a resistivity of 3.6×10^{-4} Ω cm, at a carrier concentration of 1.4×10^{20} cm^{-3}. Both the structural perfection and the electrical transport characteristics of the La-doped $BaSnO_3$ films on silicon rival those of epitaxial La-doped $BaSnO_3$ films grown on single-crystal oxide substrates.[1,2,5–7,14,22–29,82–84]

The $SrTiO_3$ buffer layer and the La-doped $BaSnO_3$ film were grown in a Veeco GEN10 dual-chamber MBE system. Each growth chamber is equipped with an *in situ* reflection high-energy electron diffraction (RHEED) system for monitoring the film growth. Substrate temperature is monitored with a thermocouple for temperatures below 500 °C and an optical pyrometer with a measurement wavelength of 980 nm for temperatures above 500 °C. The silicon substrates (2" diameter, *p*-type, boron doped, and with resistivity larger than 10 Ω cm) were cleaned in an ultraviolet ozone cleaner for 20 min before being loaded into the first growth chamber with a background pressure in the upper 10^{-9} Torr range.

An 18 nm thick $SrTiO_3$ buffer layer was grown on the bare (001) Si. The first 2 nm were grown using the epitaxy-by-periodic-annealing method[85,86] followed by an additional 16 nm grown by codeposition at 580 °C under an oxygen partial pressure of ~$(5 - 8) \times 10^{-8}$ Torr. Elemental strontium and titanium beams were generated from a conventional low-temperature effusion cell and a Ti-Ball,[87] respectively. To be specific, two 2.5 unit-cell-thick $SrTiO_3$ layers were grown by codeposition (strontium, titanium, and oxygen all supplied simultaneously) at 300 °C under an oxygen partial pressure of ~5×10^{-8} Torr, then the substrate temperature was raised to 580 °C under vacuum to enhance the crystalline quality of the as-grown $SrTiO_3$ film. After forming a 5 unit-cell-thick epitaxial $SrTiO_3$ film (i.e., two repeats of the epitaxy-by-periodic-annealing step) by this process, the substrate temperature was raised to 580 °C and additional $SrTiO_3$ was codeposited until the $SrTiO_3$ film reached a total thickness of 18 nm. RHEED patterns of the 18 nm thick $SrTiO_3$ film viewed along the [100] and [110] azimuths are shown in Figs. 1(a) and 1(b), respectively. No other phases were detected during or after the growth of the 18 nm thick $SrTiO_3$ film, indicating that the $SrTiO_3$ film is a single phase and epitaxial. More detail of the growth of the $SrTiO_3$ buffer layer on silicon is provided elsewhere.[80]

The (La-doped) $BaSnO_3$ films are grown in an adsorption-controlled regime, with molecular beams emanating from separate effusion cells containing lanthanum (99.996% purity, Ames Lab), barium (99.99% purity, Sigma-Aldrich), and SnO_2 (99.996% purity, Alfa Aesar).[2] The oxidant used for the growth of the (La-doped) $BaSnO_3$ films is a mixture of ~10% ozone and 90% oxygen. By growing $BaSnO_3$ within an adsorption-controlled regime, the stoichiometry of the $BaSnO_3$ film is ensured by exploiting the volatility of the SnO_x(g): excess

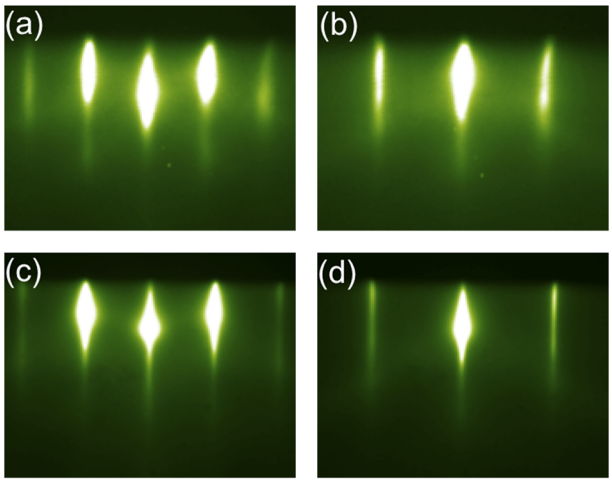

FIG. 1. RHEED patterns viewed along (a) the [100] azimuth and (b) the [110] azimuth of the 18 nm thick (001)-oriented $SrTiO_3$ buffer layer after growth. (c) RHEED patterns viewed along (c) the [100] azimuth and (d) the [110] azimuth of the overlying 318 nm thick $BaSnO_3$ film after growth.

SnO_x(g) leaves the surface of the growing film so that a stoichiometric $BaSnO_3$ film is formed.[2] During the growth of the (La-doped) $BaSnO_3$, all components—(lanthanum), barium, SnO_x, and the ~10% O_3 + 90% O_2 oxidant—are supplied simultaneously, and the substrate temperature is kept at ~700 °C. RHEED intensity oscillations (Fig. S1) were observed during the initial codeposition growth stage of the $BaSnO_3$ film on the $SrTiO_3$ buffer layer on silicon, manifesting a layer-by-layer growth mode of the $BaSnO_3$ film on $SrTiO_3$-buffered silicon at the initial growth stage.[2] A 254 nm thick undoped $BaSnO_3$ buffer layer is deposited on top of the 18 nm thick $SrTiO_3$ buffer layer, followed by a 64 nm thick active layer of La-doped $BaSnO_3$. The purpose of the thick undoped $BaSnO_3$ layer is to enhance the electron mobility of the active layer.[14,25,83] Further details on the growth of the (La-doped) $BaSnO_3$ films can be found elsewhere.[2]

RHEED patterns after the growth of the 64 nm thick La-doped $BaSnO_3$ on the 254 nm thick undoped $BaSnO_3$ buffer layer are shown in Figs. 1(c) and 1(d). The streaky RHEED patterns indicate that the surface of the La-doped $BaSnO_3$ film is epitaxial and relatively smooth on an atomic scale. The 1 × 1 surface reconstruction of the La-doped $BaSnO_3$ film observed in RHEED that is sharp and free of diffuse features manifest that the La-doped $BaSnO_3$ film is stoichiometric.[2] The surface morphology of the same sample was examined *ex situ* by atomic force microscopy (AFM) using an Asylum Research MFP-3D in tapping mode, as is shown in Fig. S2. The rms roughness of the sample is ~4 Å, which is consistent with the streaky RHEED patterns.

The crystalline quality of the same sample was assessed by *ex-situ* x-ray diffraction (XRD) with a PANalytical X'Pert system utilizing Cu $K_{\alpha 1}$ radiation. Figure 2(a) shows the θ-2θ scan of the same heterostructure characterized in Fig. 1. Only $00l$ reflections of the $SrTiO_3$ buffer layer and the $BaSnO_3$ film are observed in the θ-2θ scan, corroborating that the film is epitaxial and phase pure. A fine θ-2θ scan around the $BaSnO_3$ 002 peak is shown in Fig. 2(b). Clear thickness fringes around the $BaSnO_3$ 002 peak manifest that the interfaces of the sample are smooth. Using a Nelson-Riley analysis,[88] the out-of-plane lattice parameter of the $BaSnO_3$ film is calculated to be 4.110 ± 0.001 Å, which is close to, but slightly smaller than the bulk value of 4.116 Å.[89]

We believe the slightly smaller out-of-plane lattice parameter of the $BaSnO_3$ film is due to the tensile strain caused by the relatively large difference between the thermal expansion coefficients of $BaSnO_3$ (averaging 9.3×10^{-6} K^{-1} between room temperature to 1500 °C)[90] and silicon (averaging 3.7×10^{-6} K^{-1} between room temperature and 720 °C).[91] To verify this, we calculate the expected out-of-plane lattice parameter of the $BaSnO_3$ film at room temperature ($a^{BaSnO_3}_{out-of-plane,25\,^\circ C}$) and the expected tensile strain under the assumptions that the $BaSnO_3$ film is fully relaxed at the growth temperature (~700 °C) and that the $BaSnO_3$ film is rigidly clamped to the underlying silicon substrate as it is cooled to room temperature.

From

$$a^{BaSnO_3}_{in-plane,25\,^\circ C} - a^{BaSnO_3}_{in-plane,700\,^\circ C} = \frac{a^{silicon}_{in-plane,25\,^\circ C} - a^{silicon}_{in-plane,700\,^\circ C}}{\sqrt{2}}, \quad (1)$$

where $a^{silicon}_{in-plane,25\,^\circ C}$ = 5.4305 Å is the silicon lattice parameter at room temperature, $a^{silicon}_{in-plane,700\,^\circ C}$ = 5.444 Å is the silicon lattice parameter at the growth temperature, and $a^{BaSnO_3}_{in-plane,700\,^\circ C}$ = 4.142 Å is the in-plane lattice parameter of the $BaSnO_3$ film at the growth temperature, we can calculate the expected

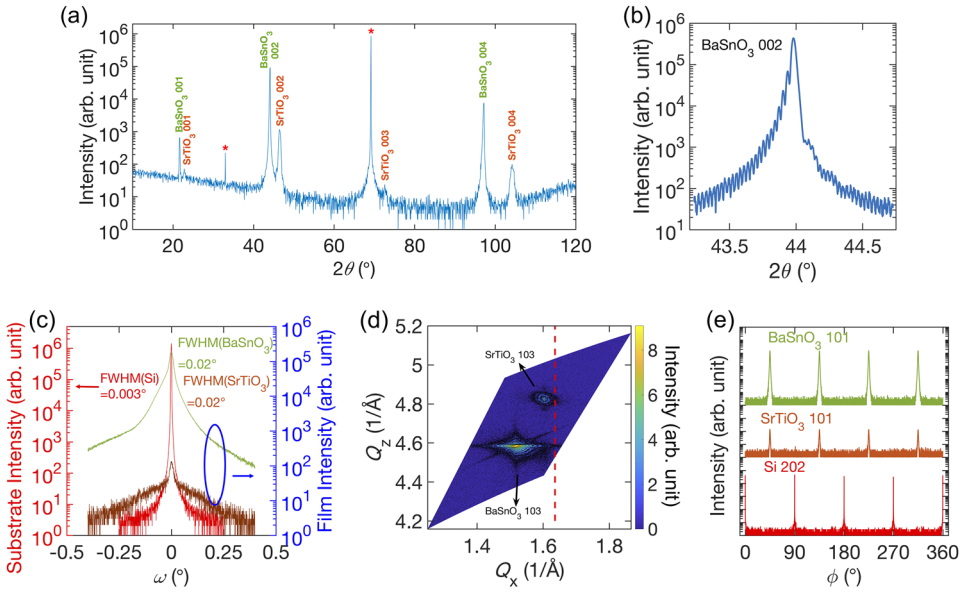

FIG. 2. (a) XRD θ-2θ scan of the same sample characterized in Fig. 1. The asterisks indicate the substrate peaks. (b) An enlarged view of the θ-2θ scan around the $BaSnO_3$ 002 peak with clear thickness fringes. The θ-2θ scan was measured with an open detector, and the fine scan around the $BaSnO_3$ 002 peak was measured in a triple-axis geometry. (c) Rocking curves of the $SrTiO_3$ and $BaSnO_3$ 002 peaks, together with that of the Si 004 peak. The FWHM of both the $SrTiO_3$ and the $BaSnO_3$ 002 peaks is 0.02°. The FWHM of the Si 004 peak is 0.003°. (d) RSM around the $BaSnO_3$ and $SrTiO_3$ 103 peaks. (e) ϕ scan of the same sample. The Si 202, $SrTiO_3$ 101, and $BaSnO_3$ 101 family of peaks were measured, and the FWHM of the film ϕ scans is 0.9° for both the $SrTiO_3$ 101 and $BaSnO_3$ 101 peaks. The ϕ scans are offset from each other along the vertical axis for clarity.

in-plane lattice parameter of the $BaSnO_3$ film, $a^{BaSnO_3}_{in-plane,25\,^\circ C}$ = 4.132 Å.

Using

$$a^{BaSnO_3}_{out-of-plane,25\,^\circ C} = \frac{2\upsilon}{\upsilon - 1} a^{BaSnO_3}_{in-plane,25\,^\circ C} + \frac{1+\upsilon}{1-\upsilon} a^{BaSnO_3}_{0,\ \ 25\,^\circ C}, \quad (2^{92,93})$$

where $a^{BaSnO_3}_{0,\ \ 25\,^\circ C}$ = 4.116 Å is the bulk lattice parameter of $BaSnO_3$, υ is Poisson's ratio of $BaSnO_3$ (here we use a value υ = 0.23 obtained from first-principles calculations),[94] we get $a^{BaSnO_3}_{out-of-plane,25\,^\circ C}$ = 4.106 Å, which is close to the out-of-plane lattice parameter we obtained from the XRD measurement (4.110 ± 0.001 Å). Note that the agreement would be improved if some relaxation occurred in the $BaSnO_3$ film as it is cooled from growth temperature to room temperature.

Using $a^{BaSnO_3}_{in-plane,25\,^\circ C}$ = 4.132 Å, we can also calculate the expected tensile strain on the $BaSnO_3$ film due to the thermal expansion difference. The expected tensile strain is 0.39%. Starting from this expected tensile strain, the expected critical thickness before mechanical cracks form can be calculated[95] using

$$h_c = \frac{a_0(1-\upsilon)^2}{5\pi \cdot f^2}, \quad (3)$$

where a_0 is the lattice parameter and f is the expected tensile strain, 0.39%. h_c is calculated to be ~1.0 μm, which is larger than the thickness of our $BaSnO_3$ film. This is consistent with our observation by AFM that our film is free of cracks.

XRD rocking curves (ω scans) of the $SrTiO_3$ and $BaSnO_3$ 002 peaks together with that of the Si 004 peak were measured in a triple-axis geometry, and the results are shown superimposed in Fig. 2(c). Despite the large ~5.4% compressive strain for (001) $BaSnO_3$ on (001) $SrTiO_3$, the crystalline quality of the $BaSnO_3$ film is similar to that of the $SrTiO_3$ buffer layer: they both have a full width at half maximum (FWHM) of 0.02° of their rocking curve, which shows a high degree of crystalline perfection for both the $SrTiO_3$ buffer layer and the $BaSnO_3$ film. This can be attributed to the optimized growth process of the $SrTiO_3$ buffer layer[80] and the adsorption-controlled growth of the $BaSnO_3$ film to maintain its stoichiometry.[2] Figure 2(d) shows reciprocal space maps (RSMs) of the $BaSnO_3$ and $SrTiO_3$ 103 peaks. The red line in Fig. 2(d) shows the film in-plane reciprocal space position that the $SrTiO_3$ and $BaSnO_3$ films would have if they were commensurately strained to the silicon substrate. Both the in-plane and out-of-plane lattice parameters of the $SrTiO_3$ buffer layer and the $BaSnO_3$ film are found to be fully relaxed to their bulk values.

If the strain introduced by defects is highly anisotropic, as is the case for our $SrTiO_3$ grown on silicon,[80] characterizing them in a single direction (the out-of-plane direction by the 002 rocking curve) is insufficient. The narrow rocking curve of the 002 $SrTiO_3$ peak is because of the insensitivity of this particular peak to threading dislocations with pure edge character.[80] This conclusion also holds for the 002 $BaSnO_3$ peak of these $BaSnO_3/SrTiO_3/Si$ films. The threading dislocation density of our $SrTiO_3/Si$ films is in excess of 10^{11} cm^{-2} (Ref. 80) and as shown below so is the threading dislocation density of the $BaSnO_3$ film grown on the $SrTiO_3/Si$. To further characterize the structural perfection of these films in a different direction (in-plane rather than out-of-plane) ϕ-scans were used. These ϕ-scans assess the in-plane mosaic spread of the $SrTiO_3$ and $BaSnO_3$ layers as well as establish their epitaxial orientation relationship. The in-plane epitaxial orientation relationship of the heterostructure was confirmed to be cube-on-cube with a 45° in-plane rotation: (001) $BaSnO_3$ ‖ (001) $SrTiO_3$ ‖ (001) Si and [100] $BaSnO_3$ ‖ [100] $SrTiO_3$ ‖ [110] Si, as is shown in Fig. 2(e). The FWHM of the film ϕ scan is 0.9° for both the $SrTiO_3$ 101 peak and the $BaSnO_3$ 101 peak. Thus, reducing the in-plane mosaic spread remains the biggest challenge to overcome for both the $BaSnO_3$ and $SrTiO_3$ layers in this heterostructure.

The microstructure of the same sample including the abruptness of the interfaces was examined by scanning transmission electron microscopy (STEM), using a probe aberration corrected Titan electron microscope operating at 300 keV. Figure 3(a) is a high-angle annular dark field (HAADF) STEM image that shows the film microstructure in cross section. Threading dislocations in the $BaSnO_3$ film are illustrated from the stripe contrast in the low-angle annular dark field (LAADF) STEM image shown in Fig. S3. The density of the threading dislocation is estimated to be ~1.3×10^{11} cm^{-2}, which is similar to the La-doped $BaSnO_3$ films grown on single-crystal oxide substrates with large lattice mismatch.[2] The threading dislocations come from both the large lattice mismatch between (001) $BaSnO_3$ and (001) $SrTiO_3$, as well as the threading dislocations from the 18 nm thick $SrTiO_3$ buffer layer on silicon.

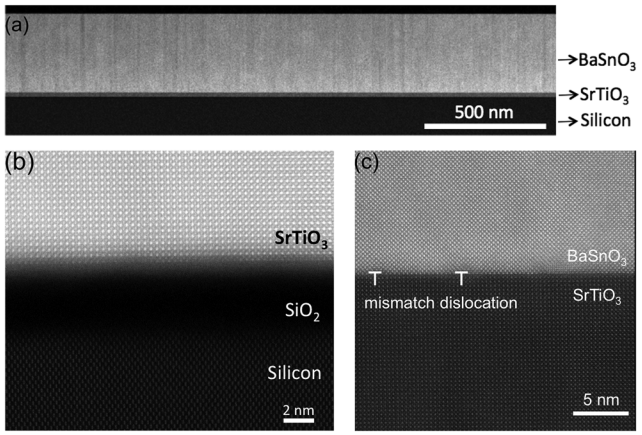

FIG. 3. STEM images showing the microstructure of the same sample characterized in Fig. 1. (a) HAADF-STEM image with a low magnification showing the overall sample. (b) The interface between the $SrTiO_3$ buffer layer and the silicon substrate shows that there is an amorphous SiO_2 layer between the $SrTiO_3$ buffer layer and the silicon substrate. (c) The interface between the $BaSnO_3$ film and the $SrTiO_3$ buffer layer is atomically sharp. Due to the large lattice mismatch between (001) $BaSnO_3$ and (001) $SrTiO_3$, there are misfit dislocations observed in the interface, two examples are marked by the edge dislocation symbols in (c).

The microstructure of the $SrTiO_3$/Si and the $BaSnO_3$/$SrTiO_3$ interfaces is shown in Figs. 3(b) and 3(c), respectively. There is a ~4 nm thick amorphous SiO_2 layer between the $SrTiO_3$ buffer layer and the silicon substrate, which originates from oxygen diffusion through the $SrTiO_3$ buffer layer during film growth. The extent of interdiffusion across the $SrTiO_3$/Si and $BaSnO_3$/$SrTiO_3$ interfaces was investigated by electron energy loss spectroscopy (EELS). As is shown in Fig. S4, there is no observable titanium interdiffusion into the SiO_2 layer. Line profiles of the elemental intensity of silicon, oxygen, and titanium across the $SrTiO_3$/Si interface are shown in Fig. S4(f). The HAADF image in Fig. 3(c) shows that the $BaSnO_3$/$SrTiO_3$ interface is abrupt and contains mismatch dislocations. The interface between the $BaSnO_3$ film and the $SrTiO_3$ buffer layer is fully relaxed, with an average spacing between edge dislocations of 22 unit cells of $SrTiO_3$ vs. 21 unit cells of $BaSnO_3$, which is consistent with the calculated ratio based on relaxed lattice parameters (~5.4%). EELS mappings of titanium and barium across the $BaSnO_3$/$SrTiO_3$ interface are shown in Fig. S5, and the corresponding line profiles shown in Fig. S5(e) also indicate a clean interface that is free of perceptible interdiffusion.

The transport properties of the same sample was measured in the van der Pauw geometry in a quantum design physical property measurement system (PPMS). Aluminum wires were wire-bonded directly to the La-doped $BaSnO_3$ film. Figure 4(a) shows the temperature-dependent resistivity. At room temperature, the resistivity is 3.6×10^{-4} Ω cm (corresponding to a conductivity of 2.8×10^3 S cm^{-1}). From 300 K to 10 K, the sample shows weak metallic behavior with no upturn of the resistivity at low temperature. The room temperature mobility of the sample is 128 cm^2 V^{-1} s^{-1}, which is comparable to most La-doped $BaSnO_3$ films grown on single-crystal oxide substrates.[1,2,5-7,14,22-29,82-84] A comparison of the room temperature mobility of our La-doped $BaSnO_3$ film on silicon with those of representative La-doped $BaSnO_3$ films grown on single-crystal oxide substrates is shown in Fig. 4(d). We attribute the high mobility of the La-doped $BaSnO_3$ film on silicon to its high degree of crystalline perfection.[11] As the temperature decreases, the mobility increases, as is shown in Fig. 4(b). At room temperature, the carrier concentration is 1.4×10^{20} cm^{-3}. From an extrapolated measurement of the lanthanum flux, made using a quartz crystal microbalance, and assuming that all of the incident lanthanum is incorporated into the La-doped $BaSnO_3$ film, the lanthanum concentration in the film is (1.6 ± 0.6)%. Comparing the lanthanum concentration to the measured concentration of mobile carriers (1.4×10^{20} cm^{-3} electrons), the dopant activation percentage is (64 ± 25)%. Figure 4(c) shows that the carrier concentration of the La-doped $BaSnO_3$ film is almost temperature independent. The temperature-dependent resistivity, mobility, and carrier concentration of our film on silicon closely resemble those of La-doped $BaSnO_3$ films grown on single-crystal oxide substrates.[1,2,5-7,14,22-29,82-84]

In summary, we have integrated La-doped $BaSnO_3$ films on silicon using an epitaxial $SrTiO_3$ buffer layer formed by MBE. The surface morphology, structural perfection, and

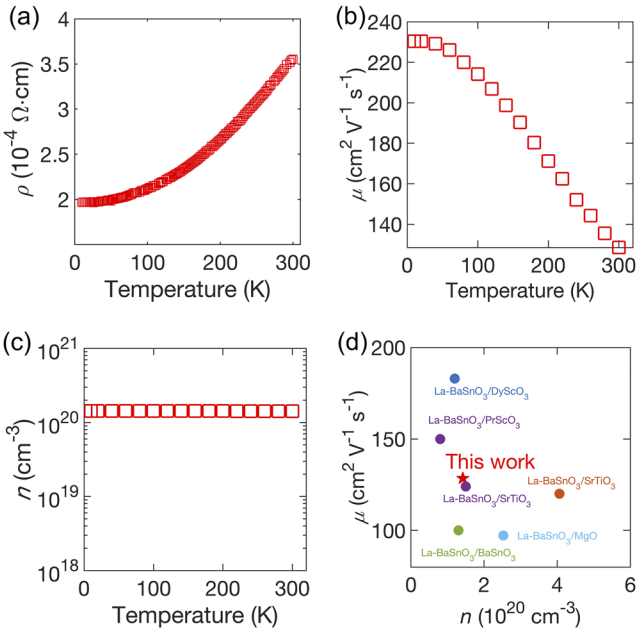

FIG. 4. Temperature-dependent (a) resistivity (ρ), (b) mobility (μ), and (c) carrier concentration (n) of the same sample characterized in Fig. 1. The results resemble those of La-doped $BaSnO_3$ films grown on single-crystal oxide substrates. (d) Comparison of the room-temperature mobility of our La-doped $BaSnO_3$ film on silicon (red star) with those of representative epitaxial $BaSnO_3$ films grown on single-crystal oxide substrates in the literature. μ is the mobility, and n is the carrier concentration of the La-doped $BaSnO_3$ films. The La-$BaSnO_3$/$DyScO_3$ data point is from Ref. 2; the La-$BaSnO_3$/$PrScO_3$ and the purple La-$BaSnO_3$/$SrTO_3$ data points are from Ref. 24; the brown La-$BaSnO_3$/$SrTO_3$ data point is from Ref. 7; the La-$BaSnO_3$/$BaSnO_3$ data point is from Ref. 26; the La-$BaSnO_3$/MgO data point is from Ref. 84.

electrical properties of our samples are similar to those of La-doped $BaSnO_3$ films grown on single-crystal oxide substrates. Our results motivate the integration of functional oxide devices utilizing the exceptional properties of $BaSnO_3$-based heterostructures (e.g., the possibility of ferroelectric field effect transistors) with the backbone of today's semiconductor industry, silicon.

See supplementary material for RHEED oscillations of $BaSnO_3$ on $SrTiO_3$ on silicon, surface morphology of the sample, and additional STEM images and EELS mappings of the sample.

This material is based on the work supported by the Air Force Office of Scientific Research under Award No. FA9550-16-1-0192. We also gratefully acknowledge the support from a GRO "functional oxides" project from the Samsung Advanced Institute of Technology. H.P., Z.C., and D.A.M. acknowledge support by the National Science Foundation [Platform for the Accelerated Realization, Analysis, and Discovery of Interface Materials (PARADIM)] under Cooperative Agreement No. DMR-1539918. This work made use of the Cornell Center for Materials Research (CCMR) Shared Facilities, which are

supported through the NSF MRSEC Program (No. DMR-1719875). Substrate preparation was performed in part at the Cornell NanoScale Facility, a member of the National Nanotechnology Coordinated Infrastructure (NNCI), which is supported by the NSF (Grant No. ECCS-1542081).

REFERENCES

[1]H. J. Kim, U. Kim, H. M. Kim, T. H. Kim, H. S. Mun, B.-G. Jeon, K. T. Hong, W.-J. Lee, C. Ju, and K. H. Kim, Appl. Phys. Express **5**, 061102 (2012).
[2]H. Paik, Z. Chen, E. Lochocki, A. Seidner H., A. Verma, N. Tanen, J. Park, M. Uchida, S. Shang, B.-C. Zhou, M. Brützam, R. Uecker, Z.-K. Liu, D. Jena, K. M. Shen, D. A. Muller, and D. G. Schlom, APL Mater. **5**, 116107 (2017).
[3]B. Ostrick, M. Fleischer, and H. Meixner, J. Am. Ceram. Soc. **80**, 2153 (1997).
[4]X. Luo, Y. S. Oh, A. Sirenko, P. Gao, T. A. Tyson, K. Char, and S.-W. Cheong, Appl. Phys. Lett. **100**, 172112 (2012).
[5]S. Ismail-Beigi, F. J. Walker, S.-W. Cheong, K. M. Rabe, and C. H. Ahn, APL Mater. **3**, 062510 (2015).
[6]W.-J. Lee, H. J. Kim, E. Sohn, H. M. Kim, T. H. Kim, K. Char, J. H. Kim, and K. H. Kim, Phys. Status Solidi A **212**, 1487 (2015).
[7]A. Prakash, P. Xu, A. Faghaninia, S. Shukla, J. W. Ager III, C. S Lo, and B. Jalan, Nat. Commun. **8**, 15167 (2017).
[8]S. Salahuddin, K. Ni, and S. Datta, Nat. Electron. **1**, 442 (2018).
[9]D. S. Ginley and C. Bright, MRS Bull. **25**, 15 (2000).
[10]H. Hosono, Thin Solid Films **515**, 6000 (2007).
[11]W.-J. Lee, H. J. Kim, J. Kang, D. H. Jang, T. H. Kim, J. H. Lee, and K. H. Kim, Annu. Rev. Mater. Res. **47**, 391 (2017).
[12]J. Li, Z. Ma, R. Sa, and K. Wu, RSC Adv. **7**, 32703 (2017).
[13]S. S. Shin, E. J. Yeom, W. S. Yang, S. Hur, M. G. Kim, J. Im, J. Seo, J. H. Noh, and S. II. Seok, Science **356**, 167 (2017).
[14]U. Kim, C. Park, T. Ha, Y. M. Kim, N. Kim, C. Ju, J. Park, J. Yu, J. H. Kim, and K. Char, APL Mater. **3**, 036101 (2015).
[15]J. Yue, A. Prakash, M. C. Robbins, S. J. Koester, and B. Jalan, ACS Appl. Mater. Interfaces **10**, 21061 (2018).
[16]K. Krishnaswamy, L. Bjaalie, B. Himmetoglu, A. Janotti, L. Gordon, and C. G. Van de Walle, Appl. Phys. Lett. **108**, 083501 (2016).
[17]A. I. Khan, K. Chatterjee, B. Wang, S. Drapcho, L. You, C. Serrao, S. R. Bakaul, R. Ramesh, and S. Salahuddin, Nat. Mater. **14**, 182 (2015).
[18]M. Suzuki, J. Ceram. Soc. Jpn. **103**, 1099 (1995).
[19]J. L. Moll and Y. Tarui, IEEE Trans. Electron Devices **10**, 338 (1963).
[20]S. Salahuddin and S. Datta, Nano Lett. **8**, 405 (2008).
[21]Y.-R. Wu and J. Singh, IEEE Trans. Electron Devices **52**, 284 (2005).
[22]H. F. Wang, Q. Z. Liu, F. Chen, G. Y. Gao, W. Wu, and X. H. Chen, J. Appl. Phys. **101**, 106105 (2007).
[23]P. V. Wadekar, J. Alaria, M. O'Sullivan, N. L. O. Flack, T. D. Manning, L. J. Phillips, K. Durose, O. Lozano, S. Lucas, J. B. Claridge, and M. J. Rosseinsky, Appl. Phys. Lett. **105**, 052104 (2014).
[24]S. Raghavan, T. Schumann, H. Kim, J. Y. Zhang, T. A. Cain, and S. Stemmer, APL Mater. **4**, 016106 (2016).
[25]J. Shiogai, K. Nishihara, K. Sato, and A. Tsukazaki, AIP Adv. **6**, 065305 (2016).
[26]W.-J. Lee, H. J. Kim, E. Sohn, T. H. Kim, J.-Y. Park, W. Park, H. Jeong, T. Lee, J. H. Kim, K.-Y. Choi, and K. H. Kim, Appl. Phys. Lett. **108**, 082105 (2016).
[27]A. Prakash, P. Xu, X. Wu, G. Haugstad, X. Wang, and B. Jalan, J. Mater. Chem. C **5**, 5730 (2017).
[28]A. V. Sanchela, M. Wei, H. Zensyo, B. Feng, J. Lee, G. Kim, H. Jeen, Y. Ikuhara, and H. Ohta, Appl. Phys. Lett. **112**, 232102 (2018).
[29]C. Shan, T. Huang, J. Zhang, M. Han, Y. Li, Z. Hu, and J. Chu, J. Phys. Chem. C **118**, 6994 (2014).
[30]K. J. Hubbard and D. G. Schlom, J. Mater. Res. **11**, 2757 (1996).
[31]D. G. Schom, C. A. Billman, J. H. Haeni, J. Lettieri, P. H. Tan, R. R. M. Held, S. Völk, and K. J. Hubbard, *Thin Films and Heterostructures for Oxide Electronics*, edited by S. B. Ogale (Springer, New York, 2005), pp. 31–78.
[32]R. A. McKee, F. J. Walker, J. R. Conner, E. D. Specht, and D. E. Zelmon, Appl. Phys. Lett. **59**, 782 (1991).
[33]M. Yoshimoto, K. Shimozono, T. Maeda, T. Ohnishi, M. Kumagai, T. Chikyow, O. Ishiyama, M. Shinohara, and H. Koinuma, Jpn. J. Appl. Phys., Part 2 **34**, L688 (1995).
[34]T. Chikyow, S. M. Bedair, L. Tye, and N. A. El-Masry, Appl. Phys. Lett. **65**, 1030 (1994).
[35]D. P. Norton, C. Park, Y. E. Lee, and J. D. Budai, J. Vac. Sci. Technol., B: Microelectron. Nanometer Struct. **20**, 257 (2002).
[36]J. Lettieri, J. H. Haeni, and D. G. Schlom, J. Vac. Sci. Technol., A **20**, 1332 (2002).
[37]S. Islam, K. R. Hofmann, A. Feldhoff, and H. Pfnür, Phys. Rev. Appl. **5**, 054006 (2016).
[38]J. H. Yum, T. Akyol, M. Lei, D. A. Ferrer, T. W. Hudnall, M. Downer, C. W. Bielawski, G. Bersuker, J. C. Lee, and S. K. Banerjee, J. Cryst. Growth **334**, 126 (2011).
[39]S. M. Lee, J. H. Yum, E. S. Larsen, W. C. Lee, S. K. Kim, C. W. Bielawski, and J. Oh, Sci. Rep. **7**, 13205 (2017).
[40]D. K. Fork, F. A. Ponce, J. C. Tramontana, and T. H. Geballe, Appl. Phys. Lett. **58**, 2294 (1991).
[41]F. Niu, A. L. Meier, and B. W. Wessels, J. Vac. Sci. Technol., B: Microelectron. Nanometer Struct. **24**, 2586 (2006).
[42]Y. Kado and Y. Arita, J. Appl. Phys. **61**, 2398 (1987).
[43]Y. Kado and Y. Arita, in *Extended Abstracts of the 20th (1988 International) Conference on Solid State Devices and Materials* (Publication Office, Business Center for Academic Society Japan, Tokyo, 1988), p. 181.
[44]D. O. Klenov, L. F. Edge, D. G. Schlom, and S. Stemmer, Appl. Phys. Lett. **86**, 051901 (2005).
[45]H. Fukumoto, T. Imura, and Y. Osaka, Appl. Phys. Lett. **55**, 360 (1989).
[46]M. Morita, H. Fukumoto, T. Imura, Y. Osaka, and M. Ichihara, J. Appl. Phys. **58**, 2407 (1985).
[47]S. Migita, Y. Morita, W. Mizubayashi, and H. Ota, in *IEEE International Electron Devices Meeting (IEDM)* (IEEE, 2010), pp. 11–15.
[48]L. F. Edge, W. Tian, V. Vaithyanathan, T. Heeg, D. G. Schlom, D. O. Klenov, S. Stemmer, J. G. Wang, and M. J. Kim, ECS Trans. **16**, 213 (2008).
[49]E. J. Tarsa, J. S. Speck, and McD. Robison, Appl. Phys. Lett. **63**, 539 (1993).
[50]J. P. Liu, P. Zaumseil, E. Bugiel, and H. J. Osten, Appl. Phys. Lett. **79**, 671 (2001).
[51]H. Nagata, M. Yoshimoto, T. Tsukahara, S. Gonda, and H. Koinuma, *Evolution of Thin-film and Surface Microstructure*, edited by C. V. Thompson, J. Y. Tsao, and D. J. Srolovitz (Materials Research Society Symposium Proceedings, 202, Pittsburgh, PA, 1991), p. 445.
[52]A. Fissel, Z. Elassar, O. Kirfel, E. Bugiel, M. Czernohorsky, and H. J. Osten, J. Appl. Phys. **99**, 074105 (2006).
[53]H. S. Craft, R. Collazo, Z. Sitar, and J. P. Maria, J. Vac. Sci. Technol., B: Microelectron. Nanometer Struct. **24**, 2105 (2006).
[54]J. Lettieri, V. Vaithyanathan, S. K. Eah, J. Stephens, V. Sih, D. D. Awschalom, J. Levy, and D. G. Schlom, Appl. Phys. Lett. **83**, 975 (2003).
[55]A. Schmehl, V. Vaithyanathan, A. Herrnberger, S. Thiel, C. Richter, M. Liberati, T. Heeg, M. Röckerath, L. F. Kourkoutis, S. Mühlbauer, P. Böni, D. A. Muller, Y. Barash, J. Schubert, Y. Idzerda, J. Mannhart, and D. G. Schlom, Nat. Mater. **6**, 882 (2007).
[56]J. Kwo, M. Hong, A. R. Kortan, K. T. Queeney, Y. J. Chabal, J. P. Mannaerts, T. Boone, J. J. Krajewski, A. M. Sergent, and J. M. Rosamilia, Appl. Phys. Lett. **77**, 130 (2000).
[57]H. J. Osten, A. Laha, M. Czernohorsky, E. Bugiel, R. Dargis, and A. Fissel, Phys. Status Solidi A **205**, 695 (2008).
[58]R. Dargis, D. Williams, R. Smith, E. Arkun, R. Roucka, A. Clark, and M. Lebby, ECS J. Solid State Sci. Technol. **1**, N24 (2012).
[59]R. Xu, Y. Y. Zhu, S. Chen, F. Xue, Y. L. Fan, X. J. Yang, and Z. M. Jiang, J. Cryst. Growth **277**, 496 (2005).

[60]T. Ji, J. Cui, Z. B. Fang, T. X. Nie, Y. L. Fan, X. L. Li, Q. He, and Z. M. Jiang, J. Cryst. Growth **321**, 171 (2011).
[61]W. Guo, A. Allenic, Y. B. Chen, X. Q. Pan, W. Tian, C. Adamo, and D. G. Schlom, Appl. Phys. Lett. **92**, 072101 (2008).
[62]M. Ishida, I. Katakabe, T. Nakamura, and N. Ohtake, Appl. Phys. Lett. **52**, 1326 (1988).
[63]H. Fukumoto, T. Imura, and Y. Osaka, Jpn. J. Appl. Phys., Part 2 **27**, L1404 (1988).
[64]J. Y. Dai, P. F. Lee, K. H. Wong, H. L. W. Chan, and C. L. Choy, J. Appl. Phys., Part 1 **94**, 912 (2003).
[65]S. Guha, N. A. Bojarczuk, and V. Narayanan, Appl. Phys. Lett. **80**, 766 (2002).
[66]G. Niu, P. Zaumseil, M. A. Schubert, M. H. Zoellner, J. Dabrowski, and T. Schroeder, Appl. Phys. Lett. **102**, 011906 (2013).
[67]V. V. Afanas'ev, S. Shamuilia, M. Badylevich, A. Stesmans, L. F. Edge, W. Tian, D. G. Schlom, J. M. J. Lopes, M. Roeckerath, and J. Schubert, Microelectron. Eng. **84**, 2278 (2007).
[68]V. V. Afanas'ev, M. Badylevich, A. Stesmans, A. Laha, H. J. Osten, A. Fissel, W. Tian, L. F. Edge, and D. G. Schlom, Appl. Phys. Lett. **93**, 192105 (2008).
[69]T. Watahiki, F. Grosse, W. Braun, V. M. Kaganer, A. Proessdorf, A. Trampert, and H. Riechert, Appl. Phys. Lett. **97**, 031911 (2010).
[70]M. Ihara, Y. Arimoto, M. Jifuku, T. Kimura, S. Kodama, H. Yamawaki, and T. Yamaoka, J. Electrochem. Soc. **129**, 2569 (1982).
[71]H. Mori and H. Ishiwara, Jpn. J. Appl. Phys., Part 2 **30**, L1415 (1991).
[72]R. A. McKee, F. J. Walker, and M. F. Chisholm, Phys. Rev. Lett. **81**, 3014 (1998).
[73]J. W. Seo, J. Fompeyrine, A. Guiller, G. Norga, C. Marchiori, H. Siegwart, and J.-P. Locquet, Appl. Phys. Lett. **83**, 5211 (2003).
[74]C. Rossel, B. Mereu, C. Marchiori, D. Caimi, M. Sousa, A. Guiller, H. Siegwart, R. Germann, J.-P. Locquet, J. Fompeyrine, D. J. Webb, Ch. Dieker, and J. W. Seo, Appl. Phys. Lett. **89**, 053506 (2006).
[75]M. Sousa, C. Rossel, C. Marchiori, H. Siegwart, D. Caimi, J.-P. Locquet, D. J. Webb, R. Germann, J. Fompeyrine, K. Babich, J. W. Seo, and Ch. Dieker, J. Appl. Phys. **102**, 104103 (2007).
[76]A. Dimoulas, G. Vellianitis, G. Mavrou, G. Apostolopoulos, A. Travlos, C. Wiemer, M. Fanciulli, and Z. M. Rittersma, Appl. Phys. Lett. **85**, 3205 (2004).
[77]S.-H. Baek and C.-B. Eom, Acta Mater. **61**, 2734 (2013).
[78]L. Zhang and R. Engel-Herbert, Phys. Status Solidi RRL **8**, 917 (2014).
[79]L. Zhang, Y. Wang, and R. Engel-Herbert, J. Appl. Phys. **119**, 045301 (2016).
[80]Z. Wang, D. Baek, B. Goodge, M. Zachman, X. Huang, X. Bai, C. M. Brooks, H. Paik, A. B. Mei, J. D. Brock, J. P. Maria, L. F. Kourkoutis, and D. G. Schlom, "Highly anisotropic distortion of epitaxial $SrTiO_3$ films on silicon due to defects," (unpublished).
[81]Y.-Y. Pai, A. Tylan-Tyler, P. Irvin, and J. Levy, Rep. Prog. Phys. **81**, 036503 (2018).
[82]H. J. Kim, U. Kim, T. H. Kim, J. Kim, H. M. Kim, B.-G. Jeon, W.-J. Lee, H. S. Mun, K. T. Hong, J. Yu, K. Char, and K. H. Kim, Phys. Rev. B **86**, 165205 (2012).
[83]C. Park, U. Kim, C. J. Ju, J. S. Park, Y. M. Kim, and K. Char, Appl. Phys. Lett. **105**, 203503 (2014).
[84]J. Shin, Y. M. Kim, Y. Kim, C. Park, and K. Char, Appl. Phys. Lett. **109**, 262102 (2016).
[85]H. Li, X. Hu, Y. Wei, Z. Yu, X. Zhang, R. Droopad, A. A. Demkov, J. Edwards, K. Moore, W. Ooms, J. Kulik, and P. Fejes, J. Appl. Phys. **93**, 4521 (2003).
[86]M. P. Warusawithana, C. Cen, C. R. Sleasman, J. C. Woicik, Y. Li, L. F. Kourkoutis, J. A. Klug, H. Li, P. Ryan, L. P. Wang, M. Bedzyk, D. A. Muller, L. Q. Chen, J. Levy, and D. G. Schlom, Science **324**, 367 (2009).
[87]C. D. Theis and D. G. Schlom, J. Vac. Sci. Technol., A **14**, 2677 (1996).
[88]J. B. Nelson and D. P. Riley, Proc. Phys. Soc. **57**, 160 (1945).
[89]F. G. Kinyanjui, S. T. Norberg, C. S. Knee, I. Ahmed, S. Hull, L. Buannic, I. Hung, Z. Gan, F. Blanc, C. P. Grey, and S. G. Eriksson, J. Mater. Chem. A **4**, 5088 (2016).
[90]T. Maekawa, K. Kurosaki, and S. Yamanaka, J. Alloys Compd. **416**, 214 (2006).
[91]Y. S. Touloukian, R. Kirby, E. Taylor, and T. Lee, *Thermophysical Properties of Matter-the TPRC Data Series*, Vol. 13, Thermal Expansion-Nonmetallic Solids (IFI/Plenum, New York, 1977).
[92]L. D. Landau and E. Lifshitz, *Theory of Elasticity*, 2nd ed., Course of Theoretical Physics Vol. 7 (Pergamon Press, 1986), p. 45.
[93]L. B. Freund and S. Suresh, *Thin Film Materials: Stress, Defect Formation and Surface Evolution* (Cambridge University Press, 2004), p. 432.
[94]A. Bouhemadou and K. Haddadi, Solid State Sci. **12**, 630 (2010).
[95]J. W. Matthews and E. Klokholm, Mater. Res. Bull. **7**, 213 (1972).

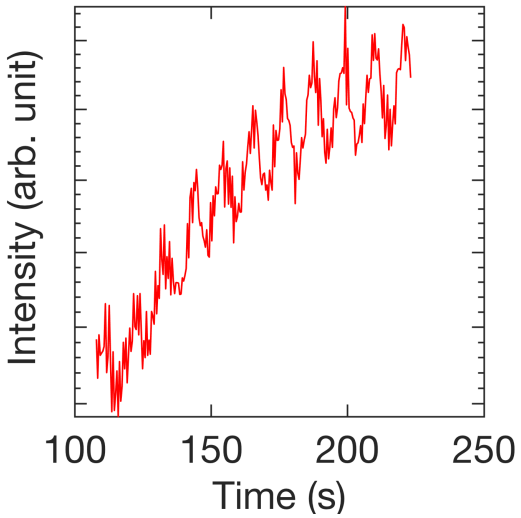

Fig. S1 RHEED oscillations of the $BaSnO_3$ film grown by codeposition during the initial growth stage on top of the 18 nm thick $SrTiO_3$ buffer layer on silicon. The oscillations indicate that the growth rate is ~0.374 Å/s.

Fig. S2 Surface morphology revealed by AFM of the same sample characterized in Fig. 1. The rms roughness is ~4 Å.

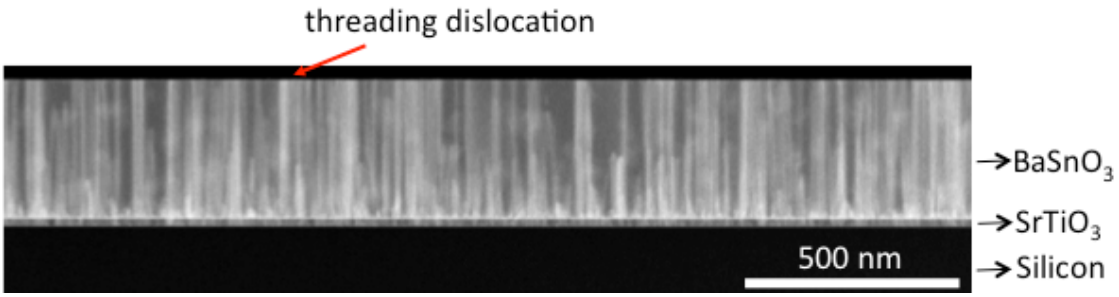

Fig. S3 LAADF-STEM image of the same sample characterized in Fig. 1 showing threading dislocations. The estimated dislocation density is ~1.3×10^{11} cm^{-2}.

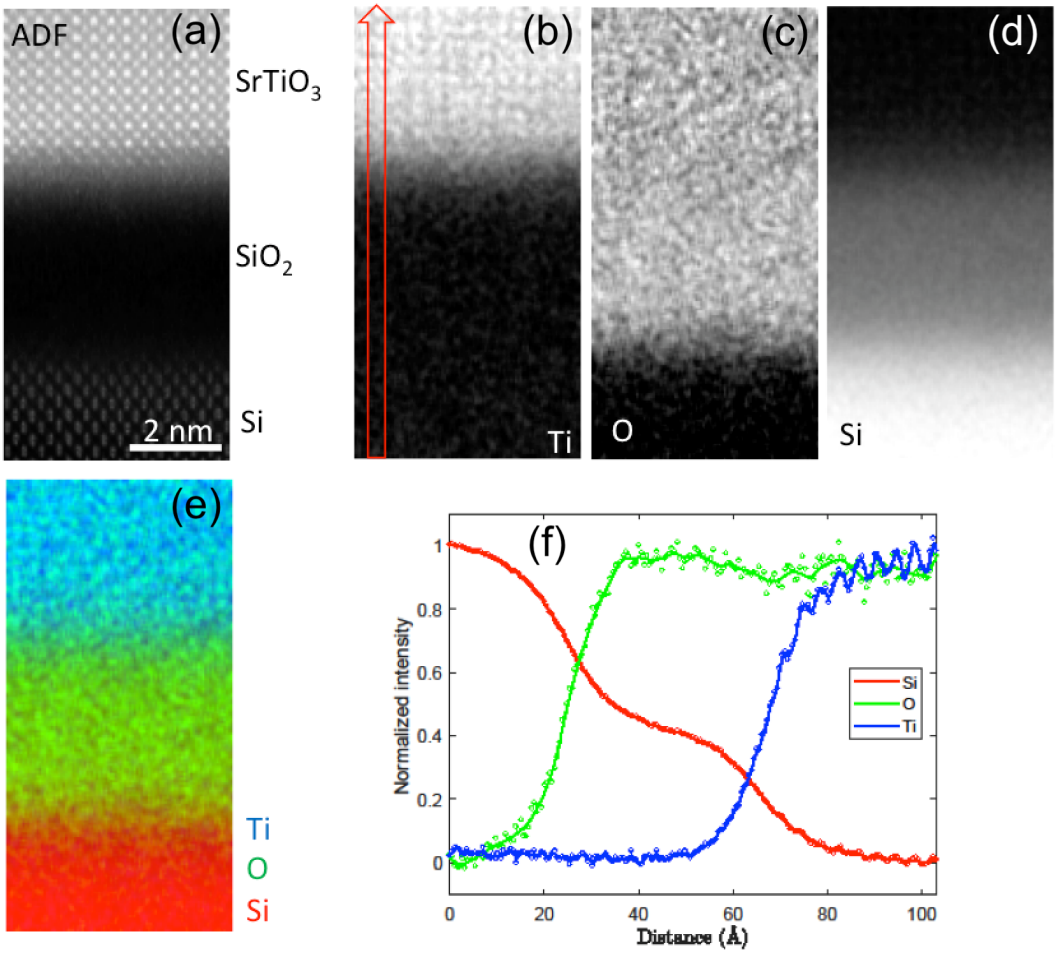

Fig. S4 (a) The HAADF-STEM image of the region in the vicinity of the $SrTiO_3$/Si interface of the same sample characterized in Fig. 1. STEM-EELS elemental maps of the same interfacial region for (b) Ti-$L_{2,3}$, (c) O-K, and (d) Si-$L_{2,3}$ edges of the same interfacial region. (e) A color-coded elemental map showing that there is no perceptible interdiffusion of titanium into the SiO_2 layer. (f) Line profiles of the elemental intensity of the same region. The zero point of the line profile in (f) corresponds to the bottom side of the arrow shown in (b).

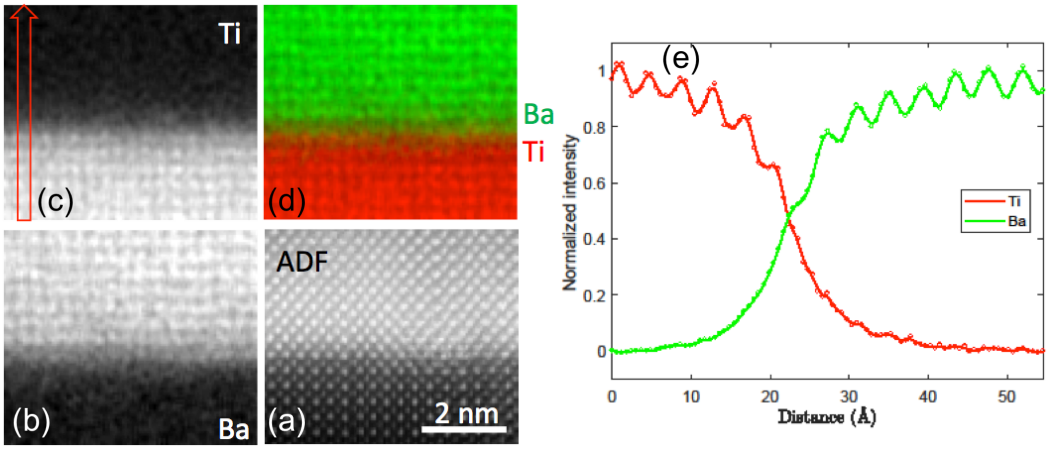

Fig. S5 (a) The HAADF-STEM image in the vicinity of the $BaSnO_3/SrTiO_3$ interface of the same sample characterized in Fig. 1. STEM-EELS elemental maps of (b) Ba-$M_{4,5}$ and (c) Ti-$L_{2,3}$ edges of the same $BaSnO_3/SrTiO_3$ interfacial region. (d) A color-coded elemental mapping showing that there is little perceptible interdiffusion of barium into the $SrTiO_3$ film. (e) Line profiles of the elemental intensity of the same region. The zero point of the line profile in (e) corresponds to the bottom side of the arrow shown in (c).